Cr-Mo-V 钢焊接接头塑性损伤的非线性超声评价

李 群[1,2], 张剑锋[1], 项延训[1], 轩福贞[1]
(1. 承压系统与安全教育部重点实验室 机械与动力工程学院 华东理工大学, 上海 200237;
2. 中石化宁波工程有限公司, 宁波 315000)

摘 要: 采用非线性超声纵波技术对汽轮机转子钢30Cr2Ni4MoV焊接接头不同程度塑性损伤试样进行了超声非线性信号的检测. 结果表明,超声非线性参数随着焊接接头试样塑性应变或损伤的加剧而显著上升; 对于同一加载情况下的试样,与母材和热影响区相比,焊缝中心的非线性参数变化最大. 同时,利用透射电子显微镜对不同塑性应变焊缝中心微观结构进行观察,发现位错密度的增加是导致非线性参数随着塑性应变增大的主要原因.

关键词: 焊接; 塑性损伤; 非线性超声; 转子钢
中图分类号: TB 115.28 **文献标识码:** A **文章编号:** 0253-360X(2014)07-0027-04

0 序 言

焊接结构广泛用于石油化工、电力和航空等领域. 焊接通常伴随着复杂物理化学反应和极其不均匀的热分布,导致材料产生缺陷、组织和力学性能的不均匀,从而使得裂纹和损伤极易从焊缝区萌生[1]. 因此,对其进行损伤检测和评定十分必要.

目前,在役焊缝结构的检测方法主要为超声检测[2,3]. 凭借其灵敏度高、穿透力强、检测速度快和对人体无害等优点,超声检测已经广泛地应用于电站[4]、压力容器[5]以及船舶行业[6]. 然而,传统线性超声(利用声速和衰减)只能检测宏观裂纹,对于材料早期损伤所产生的微裂纹和位错等变化不敏感. 最近研究表明[7-11],非线性超声技术可以克服传统线性超声的不足,对于位错和微裂纹等微组织的变化较为敏感,可用于材料的早期损伤检测,受到国内外研究者越来越多的关注.

在塑性损伤的非线性超声检测方面,Hikata 等人[7]研究了单晶铝在不同单轴拉伸或压缩塑性变形情况下二次谐波的变化情况,结果表明二次谐波幅值随变形的增加而增加. Jhang 等人[8]对 SS41 和 SS45 两种碳素结构钢不同应力加载后的试样进行非线性超声检测,结果表明非线性参量随加载应力的增大而增大. Rao 等人[9]采用纵波和瑞利波测量了不同拉伸预应变的 AA7175-T7351 铝合金试样,发现非线性参量随残余变形的增大而增大,且当变形达到一定程度后非线性参数急剧增大. Bermes[10]和 Pruell 等人[11]采用非线性 Lamb 波对不同预应变纯铝薄板试样的检测也发现了塑性损伤与非线性参数之间的关联. 尽管如此,目前有关利用非线性超声技术对复杂工程结构(如焊接接头)损伤的检测和评估尚未见报道,更多的试验工作需要开展以推进非线性超声检测技术应用于工程实际.

文中以汽轮机转子钢 30Cr2Ni4MoV 焊接接头为研究对象,通过拉伸试验获得不同程度的塑性损伤试样,进行非线性超声检测,并结合位错微观结构,分析评价焊接接头的塑性损伤.

收稿日期: 2013-01-28
基金项目: 国家高技术研究发展计划资助项目(863 计划 2012AA040106);
上海市科技启明星计划资助项目(14QA1401200)

1 超声非线性损伤检测原理

材料性能的退化通常伴随着某种非线性力学行为,即材料本构方程中产生非线性项,从而引起固体介质中传播的超声波产生高阶谐波[7-11]. 由胡克定律可知应力与应变呈非线性关系,其一维方程为

$$\sigma = E\varepsilon(1+\beta\varepsilon) \tag{1}$$

式中: σ 是轴向应力; E 是杨氏模量; β 是二阶非线性参量. 在忽略衰减的情况下,非线性波动方程的扰动解为[7]

$$\beta = \frac{8}{k^2 x}\left(\frac{A_2}{A_1^2}\right) \tag{2}$$

式中: A_1 是基波幅值; A_2 是二次谐波的幅值; x 是传播距离; $k=\omega/v$ (ω 是基波频率, v 是相速度). 由此可见非线性参数和二阶谐波位移幅值与基波位移幅值的平方之比成线性关系. 谐波的振幅取决于介质材料的性能. 因此,可以通过测量基波在介质中传

播时产生的谐波的振幅来评价介质材料的受损程度[7-12].

2 试样与检测系统

试验所用材料从转子钢 30Cr2Ni4MoV 焊接接头模拟焊件上部截取,锻件母材经过 595 ℃ ±10 ℃ 的调质处理,保温时间为 50 h,焊接后进行 580 ℃ ± 10 ℃保温时间为 10 h 的焊后热处理. 焊缝宽度大约为 20 mm,热影响区宽度大约为 2 mm. 根据 GB6397—86《金属拉伸试验试样》标准,设计试样如图 1 所示,其标距为 50 mm,截面尺寸为 9 mm × 9 mm. 利用 SANS CM75305 微机控制电子万能试验机,在应力控制的情况下,分别制作 5 个不同塑性损伤的试样,各试样的残余塑性应变分别是 0.38%, 0.45%,1.35%,1.48%和 1.82%.

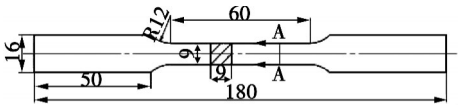

图 1 拉伸试样尺寸(mm)

Fig. 1 Schematic of tensile specimen

利用 RAM-5000 SNAP 高能超声系统对损伤试样进行检测,该系统检测示意图如图 2 所示. 采用一发一收的方式测量基波和二次谐波幅值. 超声波激励装置激发 10 个周期单频正弦波信号,加 Hanning 窗处理后经过 12db 衰减和 5 MHz 低通滤波后,驱动固定于被测试件一端的压电换能器,向试件中输入单频超声波; 位于试件另一端的压电换能器将采集到的包含有高频成分的超声波信号,经 10 MHz 高通滤波和放大后,送入信号接收器. 接收到的信号经过 FFT 变换,可得到基波和二次谐波的幅值,进

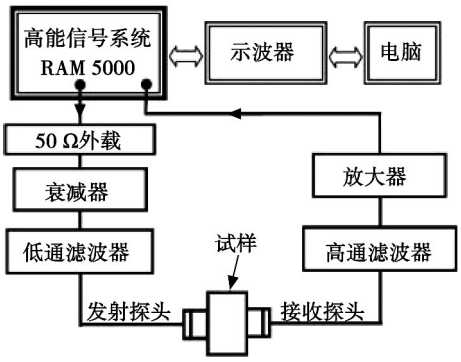

图 2 非线性超声波测量系统

Fig. 2 Schematic of experimental set-up for nonlinear ultrasonic measurement

而确定非线性参数.

采用 Olympus panametrics 系列中心频率为 5 MHz 的窄带和中心频率为 10 MHz 的宽带 PZT 超声换能器作为发射和接收传感器. 为了检测的一致性,设计了一个夹具用于固定发射换能器和接收换能器,保证检测过程中二者处于同一中心线上、且每次测量时施加在换能器上的压力相对稳定; 试样和换能器之间采用 Olympus 常温纵波耦合剂. 为了分别对焊缝、热影响区和母材进行检测,在每个试样上设置了七个检测点,如图 3 所示. 测量中每个点检测三次.

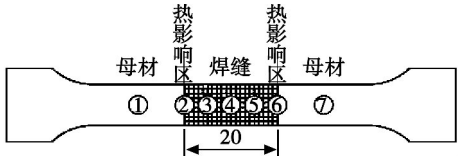

图 3 检测位置分布示意图(mm)

Fig. 3 Measurement locations on a dog-bone-shaped specimen

在对不同塑性损伤试样检测前,为了验证测量的非线性是否来自于材料本身,对不同输入电压下基波和二次谐波的幅值进行了测量. 图 4 表明在不同的衰减值下试样 1 上各个检测点处的二次谐波幅值 A_2 与基波幅值的平方 A_1^2 高度线性相关. 这表明测量的非线性来自于材料本身,与测量系统无关. 各点非线性参量存在一定的差异,这是由于焊缝材料性能的不均匀性所引起的.

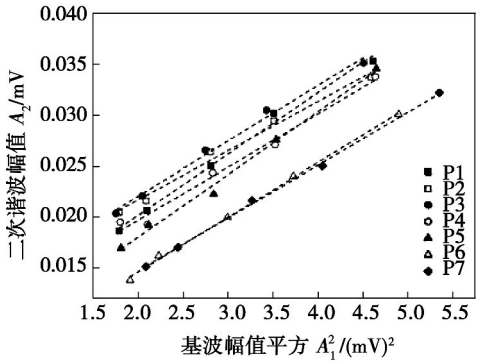

图 4 二次谐波幅值 A_2 随基波幅值平方 A_1^2 变化

Fig. 4 Variation of A_2 with A_1^2 for un-deformed specimen

3 试验结果与讨论

3.1 非线性超声检测结果

对各试样不同检测点的非线性超声检测结果如

图 5 所示. 图 5 的横坐标是检测点位置,纵坐标是指相对 0.38% 塑性应变试样的非线性参量变化率. 由图 5 可以看出母材、热影响区、焊缝三部分上的 7 个点的非线性参数 β 值的变化趋势一致,均随着应变的增大而增大,其中焊缝中心的非线性参量增加最为显著,其次是热影响区. 为了更进一步了解在不同塑性损伤情况下,焊缝中心、热影响区和母材区对于非线性超声的响应,将各区数据取均值,结果如图 6 所示. 由图 6 可以看出,焊缝中心、焊缝区、热影响区和母材区的非线性参量变化趋势基本一致,在应变为 0.45% ~1.35% 之间均存在一个平台,此间非线性参数 β 值几乎没有增长,1.35% 之后非线性参数 β 值明显增大. 另外,当塑性应变达到 1.82% 时,焊缝中心的非线性参量增加了 86%,其次是热影响区,非线性参量增加了 54%. 这说明在相同应力的拉伸作用下,焊缝中心区域和热影响区损伤最为严重.

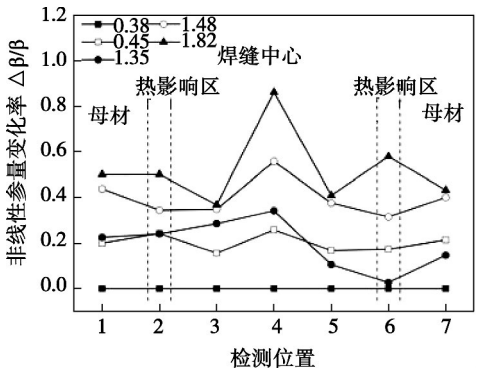

图 5　焊接接头各测量点非线性变化率结果

Fig. 5　Results of nonlinear ultrasonic on different measurement location

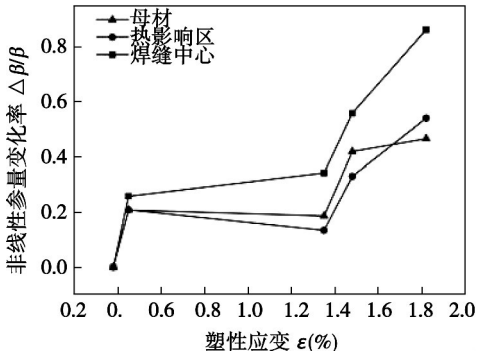

图 6　焊接接头不同区域非线性变化率随塑性应变变化曲线

Fig. 6　Variation of nonlinear ultrasonic with plastic strain in different zone of welded joint

引起汽轮机转子钢 30Cr2Ni4MoV 焊接接头各区域在相同拉伸条件下非线性超声响应不同的主要原因有以下两点: 第一,焊缝原始材料的不均匀性. 尽管汽轮机转子钢 30Cr2Ni4MoV 焊接接头是同种材料焊接,但是焊缝中心、热影响区与母材之间的力学性能与微观组织存在较大差异,这使得原始试样的非线性参量存在一定差异. 拉伸试验也表明焊缝中心材料较母材强度低. 第二,焊缝拉伸过程中塑性损伤的不均匀分布. 在相同应力拉伸的情况下,焊缝中心的塑性变形最大,因此塑性损伤最严重; 热影响区作为母材和焊缝的融合界面区,缺陷和材料的不均匀性较为集中,是焊缝结构最为薄弱的环节之一,在塑性变形中也较易产生损伤和缺陷. 检测结果符合工程实际情况.

3.2　材料位错微观结构分析

位错的形成与变化是金属材料塑性变形的典型特征[9],而且位错也是影响超声非线性的主要影响因素[7,13]. 在塑性变形过程中,位错密度的增加以及位错滑移等微观缺陷的产生,使得非线性参数随之增大. 为了了解汽轮机转子钢 30Cr2Ni4MoV 焊接接头在塑性变形过程中位错微观组织的变化,采用 TEM 技术对不同应变试样的焊缝中心位置的位错滑移进行观察. 透射电镜 TEM 试样制作的过程简述如下: 先从试样焊缝中心上割取厚度为 0.5 mm 的薄片,然后机械打磨到 100 μm,再利用双喷电解法抛光仪进行减薄至 200 nm,电解液为 10% 的高氯酸乙醇溶液,操作温度为 -10 ℃,电压为 35 V. 将制备好的样本在 PHILIPS CM200 透射电子显微镜下进行观察.

图 7 是塑性应变为 1.14% 和 3.89% 两根试样的位错形貌. 从图 7 中可以看出: 二者位错密度总体较高,位错缠绕、堆积明显; 应变为 3.89% 试样的位错密度要明显高于应变为 1.14% 试样的位错密

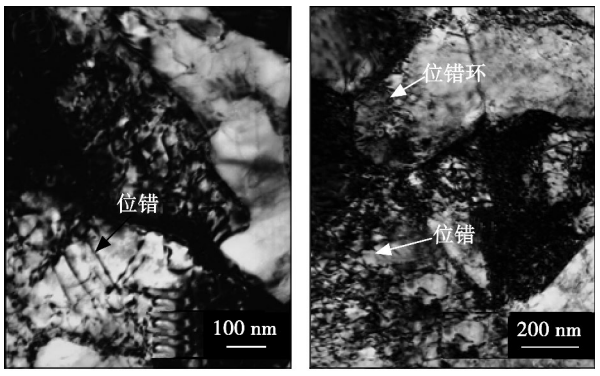

(a) 应变1.14%　　(b) 应变1.14%

图 7　30Cr2Ni4MoV 焊缝中心塑性损伤试样在透射电镜下的微观组织

Fig. 7　TEM photographs of welding center with different plastic strain

度;应变为3.89%的焊缝中心有位错环的产生. 这表明塑性变形导致汽轮机转子钢30Cr2Ni4MoV焊接接头位错密度明显增加,这也是超声非线性参量增加的主要原因.

4 结 论

(1) 超声非线性参数对汽轮机转子钢30Cr2Ni4MoV焊接接头塑性变形较为敏感,且能够有效表征焊接接头塑性变形过程中最为薄弱的区域,表明非线性超声技术可用于焊接接头早期塑性损伤的检测.

(2) 30Cr2Ni4MoV钢焊接接头塑性变形过程中导致的位错密度增加是超声非线性信号变化的主要原因.

参考文献:

[1] 周正干,滕升华,江 巍,等. 焊缝X射线检测及其结果的评判方法综述[J]. 焊接学报,2002,23(3):85-88.
Zhou Z G, Teng S H, Jiang W, *et al*. Research on defect detection and evaluation in weldS with X-rays [J]. Transactions of the China Welding Institution, 2002, 23(3): 85-88.

[2] 刚 铁,徐 艳,迟大钊,等. 铝合金焊缝超声TOFD检测的信号特征[J]. 焊接学报,2005,26(8):1-4.
Gang T, Xu Y, Chi D, *et al*. Signal characteristic of ultrasonic TOFD testing for aluminum alloy weld [J]. Transactions of the China Welding Institution, 2005, 26(8): 1-4.

[3] 陈振华,史耀武,焦标强,等. 薄镀锌钢板点焊超声谐振检测[J]. 焊接学报,2008,29(4):102-104.
Chen Z H, Shi Y W, Jiao B Q, *et al*. Ultrasonic low-frequency resonant test of spot welding of zine-coated steel sheet [J]. Transactions of the China Welding Institution, 2008, 29(4): 102-104.

[4] Ito T, Uemichi R, Tagami M, *et al*. Ido N. Ultrasonic creep damage detection by frequency analysis for boiler piping [J]. Journal of Pressure Vessel Technology, 2006, 129: 713-718.

[5] Nichols R, Crutzen S (Eds). Ultrasonic inspection of heavy section steel components: the PISC II final report [M]. London: Elsevier, 1988.

[6] Brown L M, Denale R. Real-time evaluation of ultrasonic weld inspections [C] // QNDE Programs. Review of Progress in Quantitative Nondestructive Evaluation (11). New York: Plenum Press, 1992: 1399-1406.

[7] Hikata A, Chick B B, Elbaum C. Dislocation contribution to the second harmonic generation of ultrasonic waves [J]. Journal of Applied Physics, 1965, 36(1): 229-236.

[8] Jhang K Y, Kim K C. Evaluation of material degradation using nonlinear acoustic effect [J]. Ultrasonics, 1999, 37: 39-44.

[9] Rao V V S, Kannan E., Prakash R V, *et al*. Observation of two stage dislocation dynamics from nonlinear ultrasonic response during the plastic deformation of AA7175-T7351 aluminum alloy [J]. Material Science and Engineering A, 2009, 512: 92-99.

[10] Bermes C, Kim J Y, Qu J M, *et al*. Nonlinear Lamb waves for the detection of material nonlinearity [J]. Mechanical Systems and Signal Processing, 2008, 22: 638-646.

[11] Pruell C, Kim J Y, Qu J M, *et al*. A nonlinear-guided wave technique for evaluating plasticity-driven material damage in a metal plate [J]. NDT & E International, 2009, 42: 199-203.

[12] Yost W T, Cantrell J H, Breazeale M A. Ultrasonic nonlinearity parameters and third-order elastic constants of copper between 300 and 3K [J]. Journal of Applied Physics, 1981, 52: 126-128

[13] Cantrell J H, Yost W T. Acoustic harmonic generation from fatigue-induced dislocation dipoles [J]. Philosophical Magazine A, 1994, 69(2): 315-326

作者简介: 李 群,女,1988年出生,硕士. 主要从事材料无损检测研究. Email: qunli1988@126.com

通讯作者: 轩福贞,男,博士,教授,博士研究生导师. Email: fzxuan@ecust.edu.cn

College of Electronic and Information Engineering, Nanjing University of Aeronautics and Astronautics, Nanjing 210016, China; 2. State Key Laboratory of Advanced Welding and Joining, Harbin Institute of Technology, Harbin 150001, China). pp 17 – 21, 104

Abstract: In order to further improve the accuracy and efficiency of welding defect recognition, a method was proposed to extract feature of welding defect image based on contourlet transform and kernel principal component analysis (KPCA) by chaotic particle swarm optimization (CPSO). Firstly, multi-scale decomposition of welding defect images was performed by contourlet transform. Low-frequency components and high-frequency components in a certain direction were extracted. Then, features of training samples and testing samples of welding defects were extracted using KPCA by CPSO, respectively. Finally, the type of welding defect testing samples was determined according to the Euclidean distance between features of training samples and features of testing samples. A large number of experimental results show that, compared with the feature extraction method based on KPCA and the feature extraction method based on the combination of wavelet transform and KPCA, the proposed method can extract feature more completely and has higher recognition rate and operating speed.

Key words: welding defect detection; feature extraction; contourlet transform; kernel principal component analysis; chaotic particle swarm optimization

Numerical simulation of temperature field during laser-induced welding ZHOU Guangtao[1,2], GUO Guanglei[1], FANG Hongyuan[2] (1. College of Mechanical Engineering and Automation, Huaqiao University, Xiamen 361021, China; 2. School of Materials Science and Engineering, Harbin Institute of Technology, Harbin 150001, China). pp 22 – 26

Abstract: The concept of laser-induced welding was developed and the physical and heat source model for laser-induced welding were established in this paper. The quasi-steady state equations for moving spot heat source during laser-induced welding were built. The finite element analyses were conducted through MARC software for the temperature field during laser-induced welding of 304 stainless steel. The loading of the moving spot heat source in laser-induced welding was realized based on the equations by using secondarily developed subroutine. Meanwhile, the simulated values were compared to the experimental results by measuring the thermal cycling curve of temperature filed in laser-induced welding with high temperature thermocouples. The results show that the simulated values agreed well with the measured ones.

Key words: 304 stainless steel; laser-induced; heat source model; temperature field; numerical simulation

Nonlinear ultrasonic evaluation of plastic damage for Cr-Mo-V steel welded joint LI Qun[1,2], ZHANG Jianfeng[1], XIANG Yanxun[1], XUAN Fuzhen[1] (1. Key Laboratory of Pressurized System and Safety, Ministry of Education, East China University of Science and Technology, Shanghai 200237, China; 2. Sinopec Ningbo Engineering Co., Ltd, Ningbo 315000, China). pp 27 – 30

Abstract: Nonlinear ultrasonic was used to inspect different plastic damage specimens of welded joint of steam turbine steel 30Cr2Ni4MoV. Results show that nonlinear parameter increases clearly with the plastic strain or plastic damage of specimens and the variation of nonlinear parameter of weld center is the maximum, whichis compared with the ones of the heat-affected zone and base metal under the same plastic strain condition. Moreover, it is observed that the dislocation density increases with the plastic strain in the weld center in TEM photographs, which is the primary cause to induce the increase of nonlinear parameter with the growing plastic strain.

Key words: welded joint; plastic damage; nonlinear ultrasonic; Cr-Mo-V steel

Effect of content of Ni on wettability and shear strength of BiSbSnNi solder alloy XU Yuanyuan, YAN Yanfu, FENG Lifang (College of Materials Science & Engineering, Henan University of Science & Technology, Luoyang 471000, China). pp 31 – 34

Abstract: It is one of difficult problems to research and develop the high temperature lead-free soft solder in the brazing field. Bi5Sb8Sn solder with the melting point of around 270℃ is limited because its wettability and shear strength could not meet the requirements. A new BiSbSnNi quaternary alloy was prepared by adding different content of Ni in Bi5Sb8Sn to improve the wettability and mechanical properties of Bi5Sb8Sn alloy. Results show that adding Ni makes Bi5Sb8Sn solder alloy spreadability worse than that of matrix solder. However, when the content of Ni is 2%, both the solder intermetallic compounds formation and the spreading area can increase. When the Ni content is 3%, the shear strength of the Bi5Sb8Sn3Ni alloy reaches the maximum. When the Ni content is 4%, the IMC thickness increases significantly and a lot of strip Bi phase emerges, which has an adverse effect on the shear strength of the soldered joint..

Key words: Bi5Sb8SnNi solder alloy; Ni; Wettability; Shear strength

Effect of EB off-set on joint of vanadium alloy to stainless-steel by electron beam isolation welding WANG Yarong, ZHANG Yongzhi, XU Chao, YU Yang (Institute of Machinery Manufacturing Technology, China Academy of Engineering Physics, Mianyang 621900, China). pp 35 – 38

Abstract: Vanadium alloy have been identified as leading candidate for fusion energy systems. To construct more effective and economic system, dissimilar materials joints between vanadium alloys and stainless steel were required. The high vacuum electron beam isolationwelding (EBIW) was used to joining vanadium alloy (V-5Cr-5Ti) to stainless-steel (HR-2) with the middle transition metal of Au. The effect of electron beam (EB) off-